Chemical Engineering Science 65 (2010) 2000–2008

Contents lists available at ScienceDirect

Chemical Engineering Science

journal homepage: www.elsevier.com/locate/ces

Insights into the physics of spray coating of SWNT films

Mainak Majumder [a], Clint Rendall [a], Michelle Li [a], Natnael Behabtu [a], J. Alexander Eukel [a], Robert H. Hauge [b], Howard K. Schmidt [a], Matteo Pasquali [a,b,*]

[a] Department of Chemical and Biomolecular Engineering, Rice University, USA
[b] Department of Chemistry, The Smalley Institute for Nanoscale Science and Technology, Rice University, Houston, TX-77005, USA

ARTICLE INFO

Article history:
Received 16 July 2009
Received in revised form
18 November 2009
Accepted 23 November 2009
Available online 5 December 2009

Keywords:
Carbon nanotubes
Suspension
Spray
Drop
Evaporation
Films

ABSTRACT

Spray coating is a scalable and high-throughput process for fabrication of transparent and conducting coatings (TCCs) composed of single-walled carbon nanotubes (SWNTs). Presently the fundamentals of this process are not well understood. We show that suppression of coalescence of spray droplets by sufficiently rapid heat- and mass-transfer yields homogeneous SWNT films by preventing the formation of 'coffee stains' of larger length scale. Such heat and mass transfer is driven by differential evaporation between the top and edges of the drops, whereas thermal and compositional effects on surface tension and buoyancy are weak. Ultrasonic spraying ensures that the droplets are deposited without significant splashing, and delayed splashing at higher Weber number is evidenced. We find that the performance of spray-coated TCCs made from HiPCO SWNTs is limited by bundle diameter rather than length of the constituent SWNTs and bundes. Vapor acid doping with concentrated sulfuric acid roughly doubles the conductivity of the TCCs.

1. Introduction

Thin films which are electrically conducting yet optically transparent have been employed in various applications since the last century. The first generation materials were metallic films. However these were replaced by doped semi-conducting materials since the 1950s (Haacke, 1977]) when Sn-doped In_2O_3 (or ITO—indium tin oxide) became the cornerstone of the optoelectronic and photovoltaic industry. In recent years, scarcity of In and toxicity of Sn have led to the search for alternative greener materials. Two of the most researched and prospective materials for this application are percolating networks of nanoscale conductors such as single-walled carbon nanotubes (SWNTs) (Wu et al., 2004) and doped semi-conducting zinc oxide (Rousset et al., 2009). The primary advantages of SWNT coatings over doped ZnO are that they are flexible, mechanically robust, and chemically stable (Green and Hersam, 2008). Moreover, SWNTs can serve as catalyst carriers or as catalysts themselves (Trancik et al., 2008).

Several methods of nanotube film fabrication have been reported. The most common method entails the deposition of colloidally suspended SWNTs onto porous filtration membranes (Wu et al., 2004) and subsequent transferring to other substrates (Armitage et al., 2004; Hu et al., 2004; Zhou et al., 2006). However, such processes do not scale easily. Other processes, such as flocculation of SWNT suspensions by an organic solvent (Meitl et al., 2004), drop casting from acid-SWNT dispersions (Sreekumar et al., 2003), and direct CVD growth (Ma et al., 2007) have also been explored. But they scale poorly or require special substrates. Of interest from a technology point of view are processes which are cost effective and scalable to large area and high-throughput fabrication.

Spray-coating possesses these attributes and has been adapted to synthesize transparent conductive coatings (TCC) (Kaempgen et al., 2005; Geng et al., 2007; Trancik et al., 2008; Tenant et al., 2009). Recently it has been observed that SWNT films fabricated by the spraying process have very high uniformity and smoothness (Tenant et al., 2009). Conceptually the process is simple: a colloidal suspension is sprayed uniformly over a substrate and the dispersing fluid is evaporated by heating (Pham et al., 2002), leaving the colloidal deposit to form the coating. However, this process involves heat and mass transfer at different length- and time-scales. Presently, the effect of the physics of the process on the formation, homogeneity, and properties of spray-coated SWNT TCCs is not yet understood at the fundamental level.

An integral step in the spray-coating process is the synthesis of colloidal suspensions of SWNTs. The challenge here lies in the limited dispersability of SWNTs (Vigolo et al., 2000), which are held together by strong attractive van der Waals forces. Most commonly, SWNTs are stabilized sterically or electro-statically by adsorbing surface active molecules on their sidewalls (Moore et al., 2003). Stabilization must be combined with mechanical

* Corresponding author.
E-mail address: mp@rice.edu (M. Pasquali).

0009-2509/$ - see front matter © 2009 Elsevier Ltd. All rights reserved.
doi:10.1016/j.ces.2009.11.042

debundling, usually by sonication (impingement with high-energy sound waves). However, this process also causes the longer tubes to break (Badaire et al., 2004), which is undesirable because longer SWNTs yield more conductive films (Hecht et al., 2006).

A SWNT dispersion typically consists of one-third metallic (armchair or small bandgap, few meV) and two-thirds semi-conducting (~0.5–1 eV bandgap) nanotubes. The overall conductivity of the films is limited by the presence of the semi-conducting fraction (Bernholc et al., 2002). Several compounds, either electron rich or electron deficient, are known to enhance or modulate the conductivity of carbon nanotubes, particularly by creating extra charge carriers in the semi-conducting SWNTs (Zhou et al., 2000). The most common and widely utilized are strong acids (Geng et al., 2007; [Zhou et al., 2005). Studies based on X-ray diffraction have shown that strong acids such as H_2SO_4 intercalate the bundles as anhydrous acid anions. These species form a charge transfer complex with the nanotubes and increase their electrical conductivity (Ericson et al., 2004; Zhou et al., 2005). This is the accepted molecular basis of doping of SWNT-based materials by acid. However, the effect of the doping conditions of the acids, particularly in the vapor state, can alter significantly the film properties and has not been addressed.

In this article, we measure the DC sheet conductivity and optical transparency of films and combine these properties into a single figure of merit (Dan et al., 2009). The figure of merit allows easier interpretation of the effect of the experimental parameters on the film performance as well as comparison with other candidate materials and processes. We investigate the coating formation, homogeneity, and final properties from three different types of SWNT colloidal phases: an unstable suspension of SWNT in an organic solvent, a surfactant stabilized aqueous suspension, and a surfactant/co-surfactant stabilized suspension. The footprints of the droplets are examined by optical microscopy and AFM, and an order-of-magnitude analysis is performed to understand the relative effect of the physical and chemical processes which control the formation of the coatings. The impact of preparation conditions of the SWNT suspensions—particularly sonication time—affecting the coating performance is determined, and the effect of acid doping affecting film performance is studied by Raman spectroscopy.

2. Experimental section

2.1. Synthesis and characterization of SWNT suspensions

SWNTs (HiPco, Rice University, batch #187.3) (Bronikowski et al., 2001) purified by a method described earlier (Xu et al., 2005) were utilized in this investigation. Suspensions of SWNTs in water were prepared by adding 20 mg of SWNT to 20 ml of 5 wt% SDBS solution. The suspension was homogenized for 1 h and then ultrasonicated for 5–120 min with an ultrasonic processor (CPX 600, 20 kHz, 600 W, Cole Parmer Instruments) followed by centrifugation at 10,000 rpm for 25 min to remove the large bundles of SWNTs, which constitute most of the material. It should be noted that the centrifugation step was identical for each dispersion regardless of the sonication time employed. The supernatant (concentration ~40–60 mg l^{-1}, as measured by optical absorbance at 763 nm) (Moore and Single, 2005) was used for making the films. We did not observe any systematic variation in the concentration of the SWNTs in the supernatant as a function of sonication time. SWNT–isopropyl alcohol (IPA) suspensions were prepared by adding directly ~4–5 mg of SWNTs into 100 ml of IPA and sonicating for 120 min. Triton-X/SDBS/SWNT suspensions were prepared by adding equal amounts of Triton-X-100 solution (1 g l^{-1}) and SWNT–SDBS suspension (40–60 mg l^{-1}), and then evaporating half of the water to reach a concentration of SWNTS comparable to the SWNT–SDBS suspensions. Contact angle and surface tension were measured with a CAM-200 instrument (KSV Instruments, Finland) in sessile drop and pendant drop modes, respectively. The density of each suspension was measured by weighing small samples (1–3 ml) of it. Viscosity of each suspension as a function of shear rate was measured on ARES rheometer (Rheometric Scientific).

2.2. Spray-coating apparatus, SWNT-coating fabrication and characterization

The schematic of the spray-coating apparatus is shown in Fig. 1. It consists of an ultrasonic atomizer (Model 06-5108, 120 kHz operation frequency (f), Sono-tek Corporation, NY) connected to a syringe pump, steering air to carry the droplets to the coating surface, and a hot-plate attached to a computer-controlled x–y stage (Velmex Stepping Motor Controller, Velmex Inc., NY). After fabrication, the films produced from surfactant suspensions were dipped in a 1:1 methanol/water bath heated at 60 °C for 3–4 h to remove residual surfactant and were then dried in ambient conditions.

Vapor-phase acid doping of the films was performed in a set-up shown in Fig. 1. The vapor-phase method was chosen over a liquid-phase doping technique to avoid potential mechanical damage to the film by the liquid flow.

The DC sheet resistance of the films was measured by an Alessi four-point probe apparatus, and the transparency was measured by the transmittance at 550 nm in a UV–Vis Spectrophotometer (Model UV-3101 PC, Shimadzu).

3. Results and discussion

In a homogenous film of a homogenous material, the DC sheet resistivity depends linearly on the natural logarithm of the transparency. In carbon nanotube coatings, the conductivity arises from a network of connected conducting sticks, a sharp change in the resistivity vs. log-transparency curves is often observed in experimental data, indicating loss of percolation in the network. The critical thickness (and hence conductivity and transparency) where this occurs depends on the specific composition of the material, i.e., length and diameter of the nanotube or bundles, as well as the deposition method. The quality of a film can be assessed with a single figure of merit (FOM) (Dan et al., 2009):

$$FOM = -R\ln(TR) \quad (1)$$

Here TR is a ratio. The units of resistivity determine the units of the figure of merit. Hereafter, it is reported in $\Omega\,sq^{-1}$. The merit number is useful to compare films of different thickness and therefore different conductivity and transparency. Lower merit number denotes better films. For example, typical values of conductivity of ITO films are ~28 $\Omega\,sq^{-1}$ at 90% transmittance (Yong et al., 2007), which lead to a merit number of ~3. The potential application space of the transparent conductive coatings can be assessed by using merit numbers. Transparent conductive coatings with merit numbers as large as 10^6 can be used for electrostatic dissipation, while with merit numbers approaching ~150 and ~100 are appropriate for cathode ray tubes and touch-screen applications (Kaempgen et al., 2005). Conducting films made from nano-scale conductors with merit numbers in the range 100–500 have been shown to perform with efficiencies comparable to ITO in dye sensitized solar cells (Wang et al., 2008), although films with merit numbers close to ITO (~3) are more

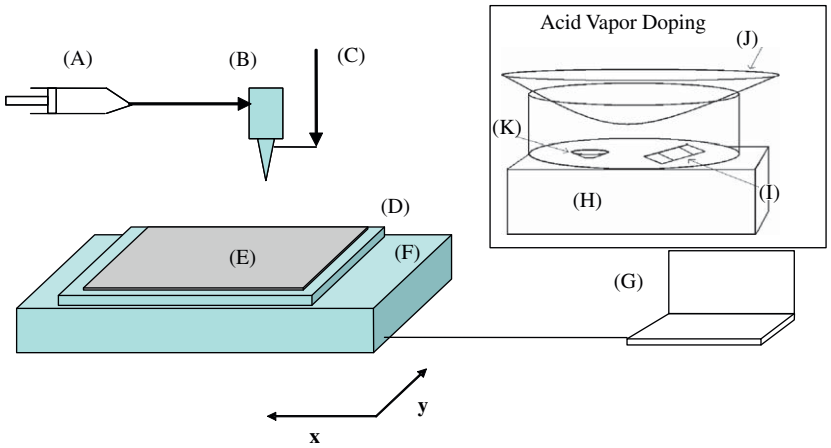

Fig. 1. Schematic of the spray-coating process. The SWNT dispersion in a syringe pump (A) is atomized by an ultrasonic droplet generator (B), (C) is the steering-air flow which forces the liquid drop to deposit on the substrate of interest. The drops are sprayed on a heated substrate (~180–200 °C) (D), kept on *x*–*y* stage (F), controlled by the computer (G), to form the coating (E). Inset: Apparatus for vapor-phase doping of SWNT films, (H) heating element, (I) CNT film, (J) cover slip on a Petri dish and (K) liquid acid.

Table 1
Summary of the physical characteristics of the SWNT suspensions, estimated droplet diameter, and experimentally obtained size of the footprint of the droplet.

Dispersion of SWNT	Surface tension (dyn/cm)	Contact angle on glass (deg.)	Density (gm/cm^3)	Estimated diameter ($D_{0.5}$) of droplet (μm)	Diameter of the footprint of dried droplet on glass (μm)
SDBS+water	25.1(±0.43)	16.5	1.22	11.2	55.12(±21.7)
SDBS+Triton-X+water	31.2(±0.21)	24.8	1.06	12.6	44.6(±15.7)
Isopropylalcohol	21.4(±0.19)	4.5	0.79	12.3	200(±92)

prevalent in solar-cell applications. A recently discovered advantage of films composed of SWNTs is that they can transmit IR part of the solar spectrum much more efficiently than ITO (Hu et al., 2009). For applications in flat panel displays and EMI shielding, more stringent requirements of merit numbers ~80 and ~10 are required (Kaempgen et al., 2005).

3.1. Spray-coating process

The spray-coating process (depicted in Fig. 1) involves several steps such as droplet generation by the ultrasonic generator, deposition of the droplets onto the substrate by the steering-air flow, and drying of the droplets on a heated substrate to form a film. The optimal speed of the *x*–*y* translation stage (~10 cm s^{-1}) was estimated by considering the heat and mass transfer from the heated substrate such that the drying time was small enough to avoid significant droplet coalescence while, at the same time, a uniform coating in the minimal number of spraying cycles is attained. Most coatings were formed by a ~12 cm zig-zag raster in the *x*-direction, followed by a ~1 cm *y*-translation and then another ~12 cm raster in the opposite *x*-direction. The coating thickness was controlled by the number of rasters. The scheme of the zig-zag raster is shown in Supplemental Section S1. Neglecting edge effects, ~12 cm^2 (12 cm × 1 cm) planar area could be coated in 1 s by the method described here. Although the coatings were produced by multiple rasters, we also studied the footprints (uniformity and diameter) of ~40–45 individual droplets (roughly circular) obtained by each single raster as a function of processing parameters.

3.2. Droplet footprints: drying time-scales and drop coalescence; splashing and deposition

The ultrasonic atomizer generates droplets of uniform size by electro-mechanical transduction of piezoelectric crystals, which provide a squeeze-mode action on liquids flowing through a metallic (Ti) capillary. The droplet size generated by this sub-MHz droplet generator can be predicted with reasonable accuracy by the following experimental correlation, which is based on the more fundamental Kelvin equation for the wavelength of the sonically generated capillary waves (Lang, 1962; Berger, 1998):

$$D_{0.5} = 0.34\left(\frac{8\pi\sigma}{\rho f^2}\right)^{1/3} \quad (2)$$

Here $D_{0.5}$ is the mean drop diameter, σ is the surface tension of the liquid, ρ is the density of the liquid, and f is the frequency of the droplet generator. Without steering air, the ultrasonic nozzle emits fine droplets, most of which never reach the substrate. Therefore, an adequate steering-air velocity (~20 l min^{-1}) was also determined. Under these conditions, the diameter of the droplets of SWNT suspension ranged from 11 to 13 μm. The measured droplet footprints ranged from ~40 to 200 μm for different SWNT suspensions (Table 1), characteristic of liquid films of 25–900 nm thickness. Clearly the more wetting (smaller contact angle) suspensions produced larger footprints, which is consistent with the observations of Qiao and Chandra (1997). The shape and size of the droplet footprints depend primarily upon drop-coalescence time-scales, the droplet spreading dictated by the wettability on the surface, drying time-scales, and splashing versus deposition of the droplets impinging on the surface by the steering-air velocity. The physics of these processes governing film formation is discussed in the subsequent sections.

Fig. 2 shows images and figure of merit of the TCCs made from IPA–SWNT, SDBS–SWNT and SDBS/Triton-X. It was hypothesized that the nanotubes in IPA without the surfactant would provide better electrical contact in the percolating network with lower FOMs. however, coatings created using IPA are substantially inferior to those created with SDBS–SWNT (FOM of 700–800 vs. 400–500, respectively) dispersions used in this study. Undisturbed IPA dispersions separate into two layers (SWNT-rich

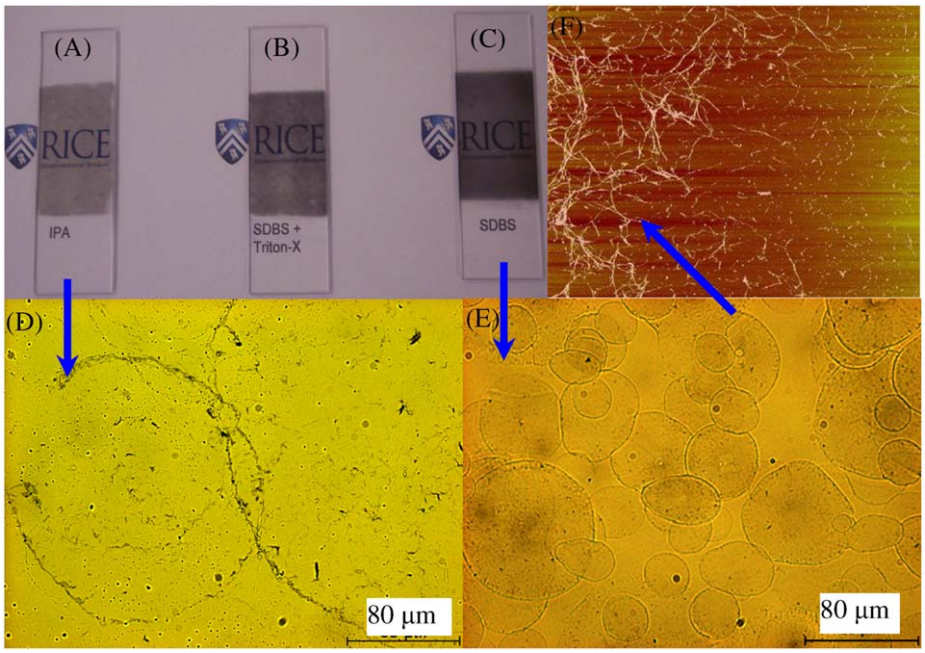

Fig. 2. Photographs of TCCs made from (A) IPA–SWNT, FOM=700; (B) SDBS–TritonX–SWNT, FOM=10,000 and (C) SDBS–SWNT, FOM=450. Optical micrograph of the footprints of (D) IPA–SWNT and (E) SDBS–SWNT spray droplets deposited on a glass substrate at elevated temperature (180–200 °C) showing coffee-stain formation at the edges of the drop. The diameter of the footprints was measured and a statistic of ~40 footprints is reported in the succeeding table. (F) AFM (height) of a 10 μm × 10 μm (scan height 50 nm) scan of the edge of a spray dried on a mica-sheet showing that some degree of alignment is provided by the flow of particles to the pinned drops.

and IPA-rich) within hours. Footprints of the droplets from IPA–SWNT suspensions (Fig. 2(D)) show significant sedimentation of particles and presence of large SWNT bundles. Conversely, SDBS–SWNT droplets form homogeneous layers (Fig. 2(E)). Therefore, the better stability of the SWNT dispersions is crucial for obtaining uniform films with superior properties. The mixture of the surfactants, SDBS and Triton-X, yielded poor results, with merit numbers on the order of 10^4 or higher after washing the surfactant, possibly because of flocculation in the suspension.

Spraying the SWNT suspension onto a room temperature substrate yielded considerable drop coalescence and therefore non-uniform films. Coalescence was suppressed by heating the substrate to 180–200 °C. Fig. 3(A) and (B) illustrates this effect. The influence of this convective heat transport in the coating formation can be assessed by defining the important dimensionless numbers (Incropera, 2007):

$$Gr = \frac{g\beta(T_s - T_\infty)L^3}{\nu^2}, \quad Ra = Gr \times Pr,$$
$$Nu = 0.54 Ra_L^{1/4}, \quad h = \frac{Nu \times k}{L} \tag{3}$$

Gr is the Grashof number, which characterizes the strength of convective flow (driven by buoyant forces due to temperature gradients) to viscous forces; *Pr* is the Prandtl number, which is the ratio of molecular diffusivity of momentum to the molecular diffusivity of heat; and *Ra* is the Rayleigh number, which characterizes the strength of convective heat transfer. *Nu* is the Nusselt number—the ratio of conductive resistance to convective thermal resistance of the liquid film. It is calculated from McAdam's correlation between *Nu* and *Ra* for the case of a hot horizontal planar surface facing upwards. Here g is the gravitational acceleration, β is the volumetric thermal expansion coefficient, ν is the kinematic viscosity of the fluid, T_S is the substrate temperature, T_∞ is the ambient temperature, and L is the length scale associated with the convective heat transfer. For the purposes of these calculations, T_s ~453 K (measured with a digital thermometer, model H12, Omega), T_∞ is ~293 K. The analysis was done for 1 s of spraying time, which corresponds to an area $A \sim 0.10\,\text{m} \times 0.01\,\text{m}$ traversed by the x–y stage. The length scale L is the ratio of the area A to the perimeter P of this spraying area. The Grashof number is $\sim 1.34 \times 10^6$. *Pr* and $g\beta/\nu^2$ are functions of fluid properties and are, respectively, ~1.72 and $\sim 8.5 \times 10^{10}\,\text{K}^{-1}\,\text{m}^{-3}$ for water at its boiling point (373 K) (Incropera, 2007). The following relations are then used to estimate the drying time of the liquid film, t_v, when heated convectively on a horizontal surface kept at elevated temperature:

$$q = hA(T_s - T_\infty), \quad \Delta H = m(c_p\,\Delta T + \Delta H_{vap}), \quad t_v = \frac{\Delta H}{q} \tag{4}$$

Here $h \sim 3000\,\text{W/m}^2\,\text{K}$ is the convective heat transfer coefficient estimated from Eq. (3), k is the thermal conductivity of the fluid, q is the heat transfer rate, A is the area involved with the heat transfer, m is the mass of fluid, ΔH is the heat required to convert vaporize the liquid, c_p is the heat capacity of the fluid, ΔT is the temperature difference between ambient and boiling point of the fluid, ΔH_{vap} is the enthalpy of vaporization of the liquid. Mass (m) is calculated from the volume of water sprayed in 1 s—about 0.0017 ml at a flow rate of $\sim 0.1\,\text{mL min}^{-1}$. The time, t_v, required to dry a thin film of the liquid convectively from the surface kept at a temperature of 453 K is estimated from Eqs. (4) and found to be ~9 ms. The heat and mass transfer correlations in (4) clearly indicate that increasing the spraying rate of the SWNT fluid or decreasing the translation speed (less area coated per unit time) increases the drying time, potentially leading to inhomogenous coatings. Experimentally, it was also observed that higher (~ten-fold) flow rates or lower coating speeds (~ten-fold) from the optimized conditions resulted in considerable drop coalescence and subsequently inhomogeneous films.

We now consider the case in which the nanotube suspensions are sprayed over the substrate at room temperature which

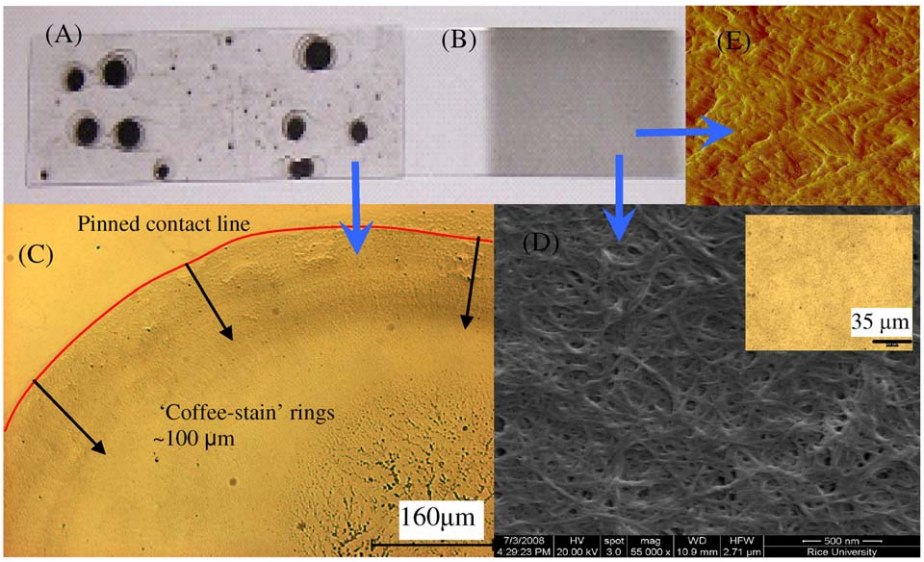

Fig. 3. Photograph of films formed by spraying at (A) room temperature and (B) at 180–200 °C. Considerable coalescence leading to formation of large droplets occurs at room temperature; while at elevated temperature the convective drying time-scale arrests the formation of large mm-scale drops. Optical image (C) showing a quadrant of an mm-scale drop after drying. Inset D: At higher temperature, the drop coalescence is arrested and a coating (scale bar is 35 μm) with a homogeneous microstructure is formed. Scanning electron micrograph (D) of the spray-coated SWNT films showing interconnected SWNT bundles and (E) is the AFM image scanned over an area 1 μm × 1 μm, height of scan 50 nm—some degree of alignment is seen.

evidently leads to the formation of inhomogenous films (see Fig. 3(A)). During evaporative drying, mass transfer from the liquid to the vapor state is substantially slower than the case of drying under convective conditions. Duggal et al. (2006) determined that, in the case of 1 μl drops of SWNTs stabilized in water by pluronic F68, with ~2 mm initial footprint radius, and at room temperature, the drying time is ~600 s and the evaporation rate is $\sim 2\times10^{-12}\,m^3\,s^{-1}$. Evaporation from a droplet is a diffusion-limited process and the rate, in general, depends linearly on the radius of the drop (Deegan et al., 2000). Therefore, the evaporation rate of a similar suspension with ~50 μm drop-footprint diameter (measured footprint diameter of SDBS–SWNT suspension on glass—see Table 1) is $\sim 2.56\times10^{-14}\,m^3\,s^{-1}$. Using a simple volumetric argument for individual spherical droplets of ~11.2 μm diameter (volume $\sim 7\times10^{-16}\,m^3$) generated by the ultrasonic generator, with similar evaporation rate at room temperature, would dry completely in ~27 ms.

It is worthwhile to compare these drying time-scales with drop-coalescence time-scale especially in this case when large areas are to be coated with multiple spray drops. The estimated time-scale $\sim(\rho D^3/8\sigma)^{1/2}$ for surface tension-driven drop coalescence (Wu et al., 2004) of ~11.2 μm pendant drops of SWNT–SDBS is in the order of microseconds. Therefore, the drying time-scale (either milliseconds for the convective drying or tens of milliseconds for evaporative drying) suggests that surface tension-driven drop coalescence during the spraying or after deposition on the substrate is faster than drying. The contact angle of the impinging droplets on the substrate also influences the droplet coalescence significantly (smaller contact angle produced larger droplet footprints—see Table 1). The relaxation speed of sessile drops on a surface has been observed to depend strongly on the contact angle and shows higher coalescing speed for lower contact angle droplets (Narhe et al., 2004). Because the diameter of the droplet footprint should be directly related to the speed of this relaxation process, our observation of the decrease in the size of the footprints with decreasing wettability of the suspension is an indication of sessile droplet coalescence on the surface. Therefore, the occurrence of sessile drop coalescence explains why the footprints of the spray droplets in the case of convective drying are significantly larger than the droplets generated by the ultrasonic generator (compare estimated diameter of droplet vs. diameter of footprint—Table 1) and also why the droplets can grow to mm-scale sizes (or larger) in the case of evaporative drying (Fig. 3(B)). Drop coalescence is followed by contact line pinning and loss of the solvent due to drying.

The microstructure of the coating evolves during the drying of the solvent, as the colloidal particles are transported to the pinned edges leading to the formation of 'coffee-rings' (Deegan et al., 2000). This particle transport mechanism is based on the differential solvent loss rates at the edges and the centers of the drops. Faster mass loss at the edges cause liquid to flow from the center to the edges and carries with itself the particles to the droplet edges (Deegan et al., 1997). However, a significant difference during drying of one-dimensional materials such as SWNTs, compared to spherical colloidal particles, is the reduced rotational mobility which tends to radially align the SWNTs at the pinned edges (Li et al., 2006). The atomic force microscope (AFM) image of the SWNT droplets dried on the mica substrate (Fig. 2(E)) shows that such ordered structures are indeed present in nano-scale domains, most likely at the edges of the drops, although such alignment is masked at the macro-scale due to overlapping droplets, and a rather inter-connected network is observed (Fig. 3(D) and (E)). Thicker rings (Fig. 3(C)) are also observed for the case of evaporative drying, as the width of the ring stains are known to follow a power-law growth with time (Deegan et al., 1997). This is in sharp contrast to the convective drying case, where a much thinner layer of deposit is formed at the edge of the drops—the process being arrested by the shorter drying time (Fig. 2(E)).

Mass transfer effects based on Marangoni flows can be active during the coating formation. Such flows can arise due to surface tension gradients generated by gradients of temperature or concentration of a surface active species. The temperature-induced Marangoni number may be estimated from

(D'Aubeterre et al., 2005)

$$Ma = \frac{\partial\sigma}{\partial T}\frac{d(T_s - T_\infty)}{\mu\alpha} \quad (5)$$

where d is the height ($\sim$0.9 μm) of the liquid film (1×10^{-9} m^3 of the coating formulation is sprayed over an area of $\sim1.1\times10^{-3}$ m^2 in 1 s), $d\sigma/dT$ for water (Savino et al., 2002) is at most 1×10^{-3} N m^{-1} K^{-1}, μ is the viscosity of the SWNT–SDBS suspension $\sim6.5\times10^{-3}$ kg m^{-1} s^{-1} (see Supplemental Section S2), α is the thermal diffusivity of water (Incropera, 2007) $\sim0.17\times10^{-6}$ m^2 s^{-1}. This leads to $Ma\sim1.63\times10^2$, while the Rayleigh number estimated from heat transfer correlations is $Ra\sim2.3\times10^6$. Marangoni flows can be competitive with convective flows when the Bond number ($Bd=Ra/Ma$) is below 1 (D'Aubeterre et al., 2005). Our estimate ($Bd=1.4\times10^4$) indicates that convection dominates over Marangoni flow. The second type of Marangoni flow, where the surface tension gradient is driven by change in concentration, is also unlikely to be significant. Although the concentration of the surfactants change during solvent drying, the surface tension of the liquid droplets should remain essentially unchanged because the concentration of surfactants at the start of the drying is already much higher than the cmc of the surfactant solution (0.07 wt%) (Miller and Neogi, 1985).

The importance of droplet splashing and deposition can be assessed through the Ohnesorge (dimensionless viscosity) and Weber (dimensionless speed) numbers. The rule of thumb is that splashing is suppressed at low Weber number (Yarin, 2006). A dimensionless value K can be derived from the characteristic Reynolds, Ohnesorge and Weber numbers for the system:

$$We = \frac{\rho D V_0^2}{\sigma}, \quad \mathrm{Re} = \frac{\rho D V_0}{\mu}, \quad Oh = \frac{We^{1/2}}{\mathrm{Re}}, \quad K = We\,Oh^{-2/5} \quad (6)$$

where D is the diameter and V_0 is the velocity of the liquid droplet.

Mundo et al. (1995) state that when $K<K_{th}$=657.48, deposition occurs instead of splashing. The air velocity in our experiments is calculated from the known flow rate (direct reading front panel flowmeter, Cole Parmer) and an estimate of the steering-air outlet nozzle diameter ($\sim$5 mm). Although the drops do not accelerate to the full air velocity, this value serves as a reasonable and conservative estimate for the purposes of the dimensionless groups. The *We* and *Re* numbers are calculated from measured SWNT–SDBS physical properties (Table 1), calculated drop diameter, and measured viscosity of the dispersion ($\sim$6.5 mPa s, Supplemental Section S2). Based on this estimation, the value of K for SDBS–SWNT droplets is $\sim$188, well below the threshold for splashing. Moreover, the optical micrographs of the footprint of the droplets of SWNT–SDBS suspensions on the glass surface show spherical shapes with smooth edges; the absence of significant sharp edges or peripheral droplets corroborates that splashing does not occur in our experimental conditions.

Using the optimal SDBS–SWNT formulation, we investigated further the possibility of splashing by increasing velocity of the steering air (thereby increasing *We*). Because droplets may coalesce during spraying, the following estimates of *We* and *K* may be low. Yet, the experiments reveal two important

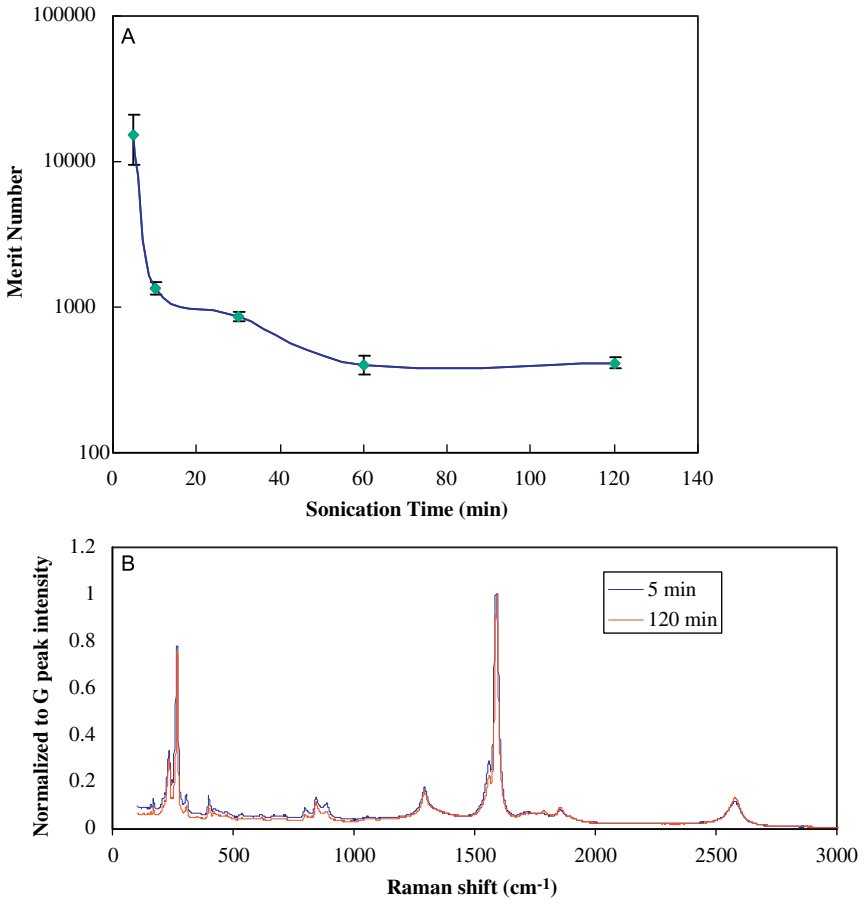

Fig. 4. (A) Effect of sonication time on the performance of the TCCs formed by the spraying process. (B) Raman spectra (using 785 nm laser) of the SWNT films made from 5 and 120 min of sonication show insignificant difference in the D_{peak}/G_{peak} ratio.

observations. Optical images of the dried footprints show no sign of splashing even when K (~1170) is significantly above transition value (see Supplemental Section S3). Moreover, the footprint of the droplets shrinks with increasing We, indicating that droplets break (likely during the flight from the nozzle to the substrate) at higher velocity, but splashing is delayed (Liu, 2000). One potential cause for delayed splashing is extensional viscosity enhancement due to the SWNTs—the phenomenon has been observed recently in samples of ~0.05 wt% of CNT in epoxy-resin (Ma et al., 2008). Recently some authors have claimed the fabrication of ultrasmooth (~3 nm rms roughness) (Tenant et al., 2009) of SWNT films using an ultrasonic spray process. It is likely that the absence of splashing as evidenced here is the reason for this important attribute.

3.2. Effect of sonication time on TCC performance

The quality of the colloidal suspension has a deep influence on the properties of the coatings. In coating fluids, the SWNTs are aggregated into bundles substantially longer and thicker than individual SWNTs. Coating fluid preparation involves sonicating the SWNTs, which at the same time break bundles but also shorten the SWNTs (Badaire et al., 2004). Hecht et al. (2006) experimentally determined the relationship between SWNT bundle length L, average diameter D_b and film electrical conductivity. Using SWNT bundles as long as 20–30 μm (individual SWNTs were ~3–4 μm in length), they observed that conductivity scales with $L^{1.46}$, i.e., longer bundles yield higher conductivity. Assuming that the nanotube junctions limit the film conductivity, the same authors predicted that the conductivity should scale as $(1/D_b^n)$, where $n \leq 2$.

We studied the effect of sonication of the SWNT colloidal suspension on the film performance. Because we used HiPco tubes (number average length ~500 nm) (Carver et al., 2005) we expect bundles shorter than those reported by Hecht et al. (2006). Fig. 4(a) shows that the figure of merit, i.e., the quality of the coatings, improves with sonication time. Raman spectra of films made with highly sonicated SWNTs show that sonication does not introduce defects in the SWNTs (the ratio of the intensity of the D_{peak} (~1290 cm^{-1}) to G_{peak} (1590 cm^{-1}) is unchanged ([Doorn et al., 2005). Because sonication simultaneously decreases the diameter and length of SWNT bundles, and because the figure of merit improves with sonication time, we conclude that the performance of spray-coated TCCs of HiPco SWNTs is limited by SWNT bundle diameter and not length.

3.3. Doping with acid vapors

After fabrication, washing of excess surfactants and acid doping substantially improves film properties. Removing surfactant by washing with alcohol–water mixtures decreases the electrical resistivity by ~1–2 orders of magnitude. The performance of the films can be further improved by doping at ~100 °C with acid vapors (97% H_2SO_4 or 37% HCl, Fisher Scientific), which decreases the resistivity (see Table 2). Surfactant removal by acid washing has been cited in the literature as likely cause for the increase in film conductivity (Geng et al., 2007). However, we find that conductivity increases by vapor doping, which cannot remove surfactant. Moreover, H_2SO_4 exposure yields comparable conductivity increase in surfactant-free films made from IPA–SWNT as well as films made from SDBS–SWNT suspensions (see Table 2). Therefore, we believe that the conductivity increase is due to the intercalation of acid molecules into SWNT bundles, as in SWNT fibers (Zhou et al., 2005). A slightly different behavior is observed for the HNO_3-doped films: HNO_3 acid-vapor treatment at RT for 6–12 h yields a ~50% decrease in resistivity—qualititatively consistent with the observations of Geng et al. (2007), but treatment at 80–100 °C increases the resistivity from ~0.4 to ~152 kΩ sq^{-1}. In these samples, Raman spectra of the treated film show higher defect density, indicated by the increase of the D_{peak}/G_{peak} ratio (Fig. 5). Conversely, H_2SO_4-vapor-doped films had low defect density (same D_{peak}/G_{peak} ratio as untreated films) and showed the best merit numbers ~95. Such films can find uses in cathode ray tubes or touch-screen applications.

4. Conclusion

In this paper, we have discussed how different physical processes act at various length- and time-scales to control the spray coating and properties of transparent, conductive SWNT films. Spray drops impinge on the coated surface without significant splashing, followed by sessile drop coalescence driven by surface tension and pinning of the edge of the drops, and finally transport of the SWNT bundles to the edges of the drops during drying of the solvent. Homogeneity in the films is attained by rapid heat and mass transfer, which suppress drop coalescence and coffee-stain formation at large length scales. During drying, SWNT bundles arrange radially with partial alignment at the edge of the droplets, but overlapping droplets mask this feature and generate a microstructure with an interpenetrating network of SWNT bundles.

The conductivity of the coatings increases (and the merit number decreases) with increasing sonication time indicating that the bundle diameter and not the bundle length is the limiting

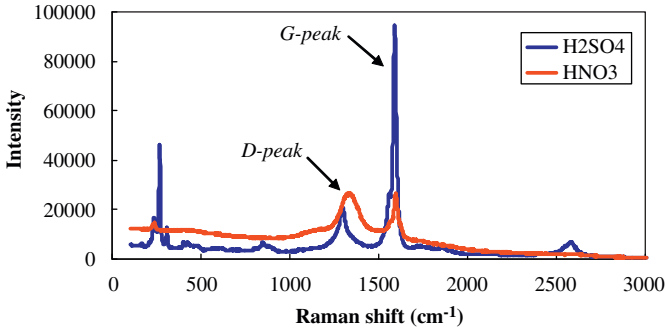

Fig. 5. Raman spectra of SWNT coatings (using 785 nm laser) with sulfuric acid and nitric acid doping.

Table 2
Summary of acid-doping studies on the electrical resistivity of the transparent conductive coatings (TCCs) carried out in the apparatus shown in inset of Fig. 1 at 80–100 °C.

Doping	Steps in fabrication	Transparency (%@550 nm)	Initial resistence (Ω sq^{-1})	Final resistence (Ω sq^{-1})	Percentage decrease (initial–final)/initial × 100
H_2SO_4	IPA dispersion	72	$2.1(\pm 0.7)\times 10^3$ FOM-689	$2.9(\pm 0.1)10^2$ FOM-95	86%
H_2SO_4	SDBS+washing	53	$7.5(\pm 0.6)\times 10^2$ FOM-476	$1.5(\pm 0.06)\times 10^2$ FOM-95	80%
HNO_3	SDBS+washing	50	$6.9(\pm 0.9)\times 10^2$ FOM-478	Very high FOM-very high	A large negative number

factor for spray-coated SWNT films made from HiPco nanotubes. Acid doping with vapors of concentrated sulfuric acid and hydrochloric acid increases the conductivity of the coatings; however, vapors of nitric acid at $\sim 100\,^{\circ}C$ degrade the properties by introducing defect sites on the SWNTs.

Although demonstrated for planar substrates, a significant advantage of spray coating could be its potential application to curved, randomly shaped or uneven surfaces. Further fundamental studies on the formation of SWNT coatings will be the key for improved processing and application of SWNT films.

Notation

TR	transparency ratio
R	sheet resistance ($\Omega\,sq^{-1}$).
D	droplet diameter (m)
f	frequency (Hz)
A	area (m^2)
P	perimeter (m)
L	characteristic length (m)
G	gravitational acceleration ($m\,s^{-2}$)
v	kinematic viscosity ($m^2\,s^{-1}$)
h	convective heat transfer coefficient ($W\,m^{-2}\,K^{-1}$)
k	thermal conductivity ($W\,m^{-1}\,K^{-1}$)
c_p	heat capacity of water ($J\,kg^{-1}\,K^{-1}$)
m	mass of water (kg)
ΔT	temperature difference between ambient and boiling point of water ~ 75 K
ΔH_v	enthalpy of vaporization ($J\,kg^{-1}$)
D	liquid film height (m)
K	splashing parameter
Q	heat transfer rate (W)
t_v	evaporation time (s)
T_S	substrate temperature (K)
T_∞	ambient temperature (K)
V_0	velocity of droplet ($m\,s^{-1}$)
Bd	bond number
Gr	Grashof number
Ma	Marangoni number
Nu	Nusselt number
Oh	Ohnesorge number
Pr	Prandtl number
Ra	Rayleigh number
Re	Reynolds number
We	Weber number

List of symbols

β	volumetric thermal expansion coefficient (K^{-1})
μ	dynamic viscosity (mPa s)
ρ	liquid density ($kg\,m^{-3}$)
σ	surface tension ($N\,m^{-1}$)

Acknowledgments

We thank Dr. Micah Green for his help with the rheological measurements, Budhadipta Dan for valuable suggestions on film making, Dr. Pradeep Bhat for discussions on splashing and deposition of droplets, Prof. Lisa Biswal for help with the contact angle and surface tension measurements, and Prof. Jim Tour for help with the electrical measurements. We gratefully acknowledge funding from the Air Force Office of Scientific Research under Grant FA9550-06-1-0207, Air Force Research Laboratory under Grant 07-S568-0042-01-C1 and US Army Corps of Engineers Environmental Quality and Installation Program under Grant W912HZ-08-C-0054.

Appendix A. Supplementary material

Supplementary data associated with this article can be found in the online version at doi:10.1016/j.ces.2009.11.042.

References

Armitage, N.P., Gabriel, J.C.P., Gruner, G., 2004. Quasi-Langmuir–Blodgett thin film deposition of carbon nanotubes. Journal of Applied Physics 95, 3228–3230.
Badaire, S., Poulin, P., Maugey, M., Zakri, C., 2004. In situ measurements of nanotube dimensions in suspensions by depolarized dynamic light scattering. Langmuir 20, 10367–10370.
Berger, H.L., 1998. Ultrasonic Liquid Atomization: Theory and Application. Partridge Hill Publishers, Hyde Park, NY.
Bernholc, J., Brenner, D., Buongiorno Nardelli, M., Meunier, V., Roland, C., 2002. Mechanical and electrical properties of nanotubes. Annual Review of Materials Research 32, 347–375.
Bronikowski, M.J., Willis, P.A., Colbert, D.T., Smith, K.A., Smalley, R.E., 2001. Gas-phase production of carbon single-walled nanotubes from carbon monoxide via the HiPco process: A parametric study, J. Vac. Sci. Technol. A 19, 1800–1805.
Carver, R.L., Peng, H., Sadana, A.K., Nikolaev, P., Arepalli, S., Scott, C.D., Billups, W.E., Hauge, R.H., Smalley, R.E., 2005. A model for nucleation and growth of single wall carbon nanotubes via the HiPco process: a catalyst concentration study. Journal of Nanoscience and Nanotechnology 5, 1035–1040.
D'Aubeterre, A., Da Silva, R., Aguilera, M.E., 2005. Experimental study on Marangoni effect induced by heat and mass transfer. International Communications in Heat and Mass Transfer 32, 677–684.
Dan, B., Irvin, G.C., Pasquali, M., 2009. Continuous and scalable fabrication of transparent conducting carbon nanotube films. ACS Nano 3, 835–843.
Deegan, R.D., Bakajin, O., Dupont, T.F., Huber, G., Nagel, S.R., Witten, T.A., 1997. Capillary flow as the cause of ring stains from dried liquid drops. Nature 389, 827–829.
Deegan, R.D., Bakajin, O., Dupont, T.F., Huber, G., Nagel, S.R., Witten, T.A., 2000. Contact line deposits in an evaporating drop. Physical Review E 62, 756.
Doorn, S.K., Zheng, L., O'Connell, M.J., Zhu, Y., Huang, S., Liu, J., 2005. Raman spectroscopy and imaging of ultralong carbon nanotubes. The Journal of Physical Chemistry B 109, 3751–3758.
Duggal, R., Hussain, F., Pasquali, M., 2006. Self-assembly of single-walled carbon nanotubes into a sheet by drop drying. Advanced Materials 18, 29–34.
Ericson, L.M., Fan, H., Peng, H., Davis, V.A., Zhou, W., Sulpizio, J., Wang, Y., Booker, R., Vavro, J., Guthy, C., Parra-Vasquez, A.N.G., Kim, M.J., Ramesh, S., Saini, R.K., Kittrell, C., Lavin, G., Schmidt, H., Adams, W.W., Billups, W.E., Pasquali, M., Hwang, W.-F., Hauge, R.H., Fischer, J.E., Smalley, R.E., 2004. Macroscopic, neat, single-walled carbon nanotube fibers. Science 305, 1447–1450.
Geng, H.-Z., Kim, K., So, K., Lee, Y., Chang, Y., Lee, Y., 2007. Effect of acid treatment on carbon nanotube-based flexible transparent conducting films. Journal of the American Chemical Society 129, 7758–7759.
Green, A., Hersam, M., 2008. Colored semitransparent conductive coatings consisting of monodisperse metallic single-walled carbon nanotubes. Nano Letters, 1417–1422.
Haacke, G., 1977. Transparent conducting coatings. Annual Review of Materials Science 7, 73–93.
Hecht, D., Hu, L., Gruner, G., 2006. Conductivity scaling with bundle length and diameter in single walled carbon nanotube networks. Applied Physics Letters 89.
Hu, L., Hecht, D.S., Gruner, G., 2009. Infrared transparent carbon nanotube thin films. Applied Physics Letters 94, 081103.
Hu, L., Hecht, D.S., Grüner, G., 2004. Percolation in transparent and conducting carbon nanotube networks. Nano Letters 4, 2513–2517.
Incropera, D., Bergman, Lavine, 2007. Fundamentals of Heat and Mass Transfer, sixth ed John Wiley & Sons.
Kaempgen, M., Duesberg, G.S., Roth, S., 2005. Transparent carbon nanotube coatings. Applied Surface Science 252, 425–429.
Lang, R.J., 1962. Ultrasonic atomization of liquids. The Journal of the Acoustical Society of America 34, 6–8.
Li, Q., Zhu, Y.T., Kinloch, I.A., Windle, A.H., 2006. Self-organization of carbon nanotubes in evaporating droplets. Journal of Physical Chemistry B 110, 13926–13930.
Liu, H., 2000. Science and Engineering of Droplets: Fundamentals and Applications. William Andrew Publishing, LLC, Norwich, New York, USA.
Ma, A., Mackley, M., Chinesta, F., 2008. The microstructure and rheology of carbon nanotube suspensions. International Journal of Material Forming 1, 75–81.
Ma, W., Song, L., Yang, R., Zhang, T., Zhao, Y., Sun, L., Ren, Y., Liu, D., Liu, L., Shen, J., Zhang, Z., Xiang, Y., Zhou, W., Xie, S., 2007. Directly synthesized strong, highly conducting, transparent single-walled carbon nanotube films. Nano Letters 7, 2307–2311.

Meitl, M.A., Zhou, Y., Gaur, A., Jeon, S., Usrey, M.L., Strano, M.S., Rogers, J.A., 2004. Solution casting and transfer printing single-walled carbon nanotube films. Nano Letters 4, 1643–1647.

Miller, C.A., Neogi, P., 1985. Interfacial Phenomena. Marcel Dekker.

Moore, V.C., 2005. Single walled carbon nanotubes: suspension in aqueous/surfactant media and chirality controlled synthesis on surfaces. PhD dissertation, Rice University.

Moore, V.C., Strano, M.S., Haroz, E.H., Hauge, R.H., Smalley, R.E., Schmidt, J., Talmon, Y., 2003. Individually suspended single-walled carbon nanotubes in various surfactants. Nano Letters 3, 1379–1382.

Mundo, C., Sommerfeld, M., Tropea, C., 1995. Droplet-wall collisions: experimental studies of the deformation and breakup process. International Journal of Multiphase Flow 21, 151–173.

Narhe, R., Beysens, D., Nikolayev, V.S., 2004. Contact line dynamics in drop coalescence and spreading. Langmuir 20, 1213–1221.

Pham, A.-Q., Glass, R.S., Lee, H.T., 2002. US Patent 6,358,567 B2, USA, vol. US.

Qiao, Y.M., Chandra, S., 1997. Experiments on adding a surfactant to water drops boiling on a hot surface. Proceedings: Mathematical. Physical and Engineering Sciences 453, 673–689.

Rousset, J., Saucedo, E., Lincot, D., 2009. Extrinsic doping of electrodeposited zinc oxide films by chlorine for transparent conductive oxide applications. Chemistry of Materials 21, 534–540.

Savino, R., Paterna, D., Favaloro, N., 2002. Buoyancy and Marangoni effects in an evaporating drop. Journal of Thermophysics and Heat Transfer 16.

Sreekumar, T.V., Liu, T., Kumar, S., Ericson, L.M., Hauge, R.H., Smalley, R.E., 2003. Single-wall carbon nanotube films. Chemistry of Materials 15, 175–178.

Tenant, R.C., Teresa, M.B., Jeremy, D.B., Andrew, J.F., Bobby, T., Lynn, M.G., Michael, J.H., Jeffrey, L.B., 2009. Ultrasmooth, large-area high-uniformity conductive transparent single-walled-carbon-nanotube films for photovoltaics produced by ultrasonic spraying. Advanced Materials 21, 1–7.

Trancik, J.E., Barton, S.C., Hone, J., 2008. Transparent and catalytic carbon nanotube films. Nano Letters, 982–987.

Vigolo, B., Penicaud, A., Coulon, C., Sauder, C., Pailler, R., Journet, C., Bernier, P., Poulin, P., 2000. Macroscopic fibers and ribbons of oriented carbon nanotubes. Science 290, 1331–1334.

Wang, X., Zhi, L., Mullen, K., 2008. Transparent, conductive graphene electrodes for dye-sensitized solar cells. Nano Letters 8, 323–327.

Wu, M., Cubaud, T., Ho, C.-M., 2004. Scaling law in liquid drop coalescence driven by surface tension. Physics of Fluids 16, L51–L54.

Wu, Z., Chen, Z., Du, X., Logan, J.M., Sippel, J., Nikolou, M., Kamaras, K., Reynolds, J.R., Tanner, D.B., Hebard, A.F., Rinzler, A.G., 2004. Transparent, conductive carbon nanotube films. Science 305, 1273–1276.

Wu, Z.C., Chen, Z.H., Du, X., Logan, J.M., Sippel, J., Nikolou, M., Kamaras, K., Reynolds, J.R., Tanner, D.B., Hebard, A.F., Rinzler, A.G., 2004. Transparent, conductive carbon nanotube films. Science 305, 1273–1276.

Xu, Y.Q., Peng, H., Hauge, R.H., Smalley, R.E., 2005. Controlled multistep purification of single-walled carbon nanotubes. Nano Letters 5, 163–168.

Yarin, A.L., 2006. Drop impact dynamics: splashing, spreading, receding, bouncing. Annual Review of Fluid Mechanics 38, 159–192.

Yong, T.Y., Tou, T.Y., Yow, H.K., Safran, G., 2007. Pulsed Nd:YAG laser deposition of indium tin oxide thin films in different gases and organic light emitting device applications. Thin Solid Films 516, 4267–4271.

Zhou, C., Kong, J., Yenilmez, E., Dai, H., 2000. Modulated chemical doping of individual carbon nanotubes. Science 290, 1552–1555.

Zhou, W., Fischer, J.E., Heiney, P.A., Fan, H., Davis, V.A., Pasquali, M., Smalley, R.E., 2005. Single-walled carbon nanotubes in superacid: X-ray and calorimetric evidence for partly ordered H_2 SO_4. Physical Review B 72, 045440.

Zhou, Y., Hu, L., Grüner, G., 2006. A method of printing carbon nanotube thin films. Applied Physics Letters 88, 123109.